Nuclear Engineering and Design 379 (2021) 111223

Contents lists available at ScienceDirect

Nuclear Engineering and Design

journal homepage: www.elsevier.com/locate/nucengdes

Validation of a morphology adaptive multi-field two-fluid model considering counter-current stratified flow with interfacial turbulence damping

Matej Tekavčič[a,b,*], Richard Meller[b], Fabian Schlegel[b]

[a] Reactor Engineering Division, Jožef Stefan Institute, Jamova cesta 39, 1000 Ljubljana, Slovenia
[b] Institute of Fluid Dynamics, Helmholtz-Zentrum Dresden-Rossendorf, Bautzner Landstrasse 400, 01328 Dresden, Germany

ARTICLE INFO

Keywords:
stratified flow
CFD
two-fluid model
turbulence damping

ABSTRACT

Stratified flows are one of the most important multiphase flow regimes for safety analyses of the loss-of-coolant accident in pressurized water reactors. The present paper considers simulations of an isothermal counter-current stratified flow case in the channel of the WENKA (Water Entrainment Channel Karlsruhe) experiment using a morphology adaptive multi-field two-fluid modelling framework. A consistent momentum interpolation approach is applied together with the partial elimination algorithm, as it is required for strong momentum coupling, which enforces the no-slip condition at the interface and mirrors the behaviour of a homogeneous model. To model the turbulent flow conditions near an interface, the framework is extended with a turbulence damping model based on the damping scale formulation from the literature, which is introduced into the k-ω SST (Shear Stress Transport) turbulence model. The presented modelling approach is validated with experimental data for the pressure difference and vertical profiles of volume fraction, velocity and turbulent kinetic energy. Results of a mesh sensitivity study of the model are presented. Simulations were performed on two- and three-dimensional models of the channel geometry. Two turbulence damping strategies are investigated: symmetric, with damping in both phases, and asymmetric with damping only in the gas phase. The comparison shows that the asymmetric approach offers improved prediction of turbulent kinetic energy on the liquid side of the interface, but with a cost of diminished accuracy of the predicted velocity profiles on the gas side.

1. Introduction

During a hypothetical loss-of-coolant accident scenario in pressurized water reactor, part of the liquid coolant inventory may evaporate, due to partial loss of pressure in the system, and a stratified two-phase flow of steam and water can be present in a partially uncovered cold leg (Lucas et al., 2009). When the emergency core cooling system is activated to prevent a core damage due to overheating, the injection of cold water into stratified flow is related to two important safety concerns: the pressurized thermal shock (Lucas et al., 2009; Bestion, 2012), and the formation of a condensation induced water hammer (Kirsner, 1999; Barna et al., 2010). Both phenomena cause significant thermal and mechanical loads on the components of the primary cooling system which can result in damage of the reactor vessel. In both cases, safety analyses rely on good knowledge of turbulent heat and mass transfer near the interface in stratified flows (Lucas et al., 2009; Bestion, 2012; Apanasevich, 2019).

An experimental reproduction and observation of complex multiphase phenomena on realistic reactor scales and accident conditions tends to be difficult (if not impossible); therefore, computational fluid dynamics (CFD) simulations are becoming an increasingly important analytical tool in the research of nuclear reactor safety (Lucas et al., 2009; Bestion, 2012; Bestion, 2014; Höhne and Porombka, 2018). The long-term objective of our present work is to advance the capabilities of modelling tools towards the simulations of two-phase flow phenomena under realistic reactor conditions.

Many different two-phase flow phenomena, such as bubbles, large waves, slugs, droplets, thin films, etc., can co-exist in realistic turbulent two phase flows. With a typically large surface area of finely dispersed interfaces and a diverse range of physical scales with different interface morphologies involved, it can be very impractical and time consuming to use one of the precise interface tracking methods for direct resolution

* Corresponding author at: Reactor Engineering Division, Jožef Stefan Institute, Jamova cesta 39, 1000 Ljubljana, Slovenia.
E-mail address: matej.tekavcic@ijs.si (M. Tekavčič).

https://doi.org/10.1016/j.nucengdes.2021.111223
Received 11 December 2020; Received in revised form 24 March 2021; Accepted 28 March 2021
Available online 28 April 2021

of all these interfaces (Štrubelj and Tiselj, 2010).

Simulations with the two-fluid approach (Euler-Euler) for modelling of the two-phase flow and the Unsteady Reynolds Averaged Navier–-Stokes (URANS) method for turbulence modelling are the most appropriate tools for simulations of realistic industrial size applications. However, such two-fluid models were primarily developed to simulate dispersed two-phase flows. For flows where large (resolvable) interfaces are present, such as in stratified flows, an interface tracking method has to be added into the two-fluid model formulation in a so-called hybrid modelling approach (Štrubelj and Tiselj, 2010).

The *morphology adaptive multi-field two-fluid model* (from now on referred to as the *hybrid model*) used in the present work represents one such hybrid approach, which was developed by Meller et al. (2020) using the open sourceC++ library OpenFOAM. The solver is based on the GENTOP concept of Hänsch et al. (2012) with the idea to model different flow morphologies as multiple numerical continuous and dispersed phases within a unified framework (Meller et al., 2020). For numerical accuracy and robustness, the solver also features a consistent momentum interpolation (Cubero et al., 2014) with the partial elimination algorithm (Spalding, 1981) to handle the strong interphase drag coupling at a resolved interface. Both numerical procedures of the solver are described in greater detail in the paper of Meller et al. (2020). The hybrid model (Meller et al., 2020) is being developed with the long-term goal to simulate complex industrial scale multiphase flows. However, the interactions between a complex set of required models and their effects on the solution are often very difficult to determine. During model development, the best approach is to focus on one modelling aspect only with a separate model validation on simpler cases. The focus of the present paper is on modelling of turbulence near the gas–liquid interface in stratified flows.

The present paper considers the simulation of an isothermal stratified counter-current flow of air and water in the rectangular channel test section of the WENKA experiment (Stäbler et al., 2006; Stäbler, 2007). A supercritical stratified flow was chosen as validation case for the presented modelling approach. The Froude number is 2.36 and Reynold numbers are 12000 and 27000 for water and air, respectively.

In the recent years it has been well established, that special treatment is required for turbulent quantities near a free-surface in multiphase RANS turbulence modelling (Frederix et al., 2018; Höhne and Porombka, 2018; Fulgosi et al., 2003; Egorov, 2004; Porombka and Höhne, 2015). As shown by Fulgosi et al. (2003), the turbulence in the gas phase is dampened near the gas–liquid interface, similar to a solid wall boundary. To address this, Egorov (2004) proposed to add additional turbulence damping terms into the ω equation of the k-ω RANS model, which ensures a high turbulence dissipation rate (ω) at the interface and thus lowers the turbulent kinetic energy (k) at this location.

Porombka and Höhne (2015) simulated the stratified flow in the WENKA experimental facility using the two-fluid model with the Algebraic Interfacial Area Density (AIAD) model with flow morphology detection implemented into the CFD software ANSYS CFX. They derived a large interface drag model from a local shear stress formulation, thus avoiding limitations of experimental correlations. They also demonstrated that turbulence damping (with the Egorov, 2004 model) at a free-surface is necessary to reproduce experimental data.

Following up, Höhne and Porombka (2018) presented simulation results of the WENKA experiment with an sub-grid wave turbulence model, which generates additional turbulent kinetic energy at a free surface, due to sub-grid waves from the occurring Kelvin–Helmholtz instability. However, they also reported that for the chosen flow conditions, which are also considered in the present work, the effect of such a model is very small, which is in agreement with rippled flow regime observed in the experiment.

Frederix et al. (2018) presented a modified turbulence damping model derived in terms of turbulence damping scale, which produces less grid dependent results, compared to the original formulation by Egorov (2004), for simulations of a turbulent co-current stratified flow from experiments of Fabre et al. (1987). The damping scale model was also used in a "hybrid dispersed-large interface solver" presented by Mathur et al. (2019), who used it to simulate the same Fabre channel experiment (Fabre et al., 1987), among other multiphase regime cases. They also noted the importance of turbulence damping to match the experimental observations.

The main goal of the present paper is to demonstrate the capability of the hybrid model (Meller et al., 2020) to simulate stratified flows with the focus on URANS turbulence modelling near the large well defined gas–liquid interface. For this purpose, the solver capabilities are extended to account for turbulence damping near an interface and are based on the damping scale formulation of Frederix et al. (2018), which is introduced into the k-ω SST (Shear Stress Transport) turbulence model (Menter et al., 2003), as presented in Section 2. Validation of the modelling approach with measurements from WENKA experiment (Stäbler, 2007) is presented in the last Section 3. A parametric study on the damping scale modelling parameter and mesh sensitivity study are performed. The present study includes an asymmetric damping approach with either no turbulence damping in the liquid phase, or weaker damping in the liquid compared to the gas phase.

2. Numerical simulation

The open sourceC++ library OpenFOAM was used to perform simulations using the hybrid two-fluid model (Meller et al., 2020; Schlegel et al., 2021; Hänsch et al., 2021). The framework consists of the averaged equations of the two-fluid model for multiple phases, including closure relations for interphase momentum transfer, as described in the next Sections. The solver numerical procedure is based on finite volume discretization, uses consistent momentum interpolation (Cubero et al., 2014) and features the partial elimination algorithm (Spalding, 1981), which is necessary to properly handle the strong momentum coupling between the phases at a large interface. In the present work, the turbulence damping scale model of Frederix et al. (2018) is adapted to the utilized multiphase framework. In Meller et al. (2020) the model is formulated for an arbitrary number of continuous and dispersed phases. For the sake of clarity, some of the model equations are simplified to the system of two continuous phases: air and water.

2.1. Basic equations

Isothermal and incompressible two-phase flows of gaseous air (g) and liquid water (l) are modelled by mass and momentum conservation equations of the two-fluid model (Ishii and Hibiki, 2006)

$$\frac{\partial \alpha_k}{\partial t} + \boldsymbol{u}_k \cdot \nabla \alpha_k = 0 \ , \tag{1}$$

$$\frac{\partial(\alpha_k \rho_k \boldsymbol{u}_k)}{\partial t} + \nabla\cdot(\alpha_k \rho_k \boldsymbol{u}_k \boldsymbol{u}_k) = \nabla\cdot\mathbf{T}_k - \alpha_k \nabla p + \alpha_k \rho_k \boldsymbol{g} + \boldsymbol{M}_k \ . \tag{2}$$

Sub-scripted quantities $\alpha_k, \rho_k, \boldsymbol{u}_k$ indicate the phase fraction, density and velocity of phase k, respectively. The terms $\mathbf{T}_k$ and $\boldsymbol{M}_k$ represent the effective stress tensor and momentum sources due to phase interaction, respectively. Pressure p is shared by both phases and $\boldsymbol{g}$ marks the gravitational acceleration. The phase fractions are related to each other as $\alpha_g + \alpha_l = 1$.

The effective stress tensor $\mathbf{T}_k$ combines viscous stress $\mathbf{T}_k^{\mu}$ and turbulent stress $\mathbf{T}_k^{\mathrm{T}}$ so that

$$\mathbf{T}_k = \mathbf{T}_k^{\mu} + \mathbf{T}_k^{\mathrm{T}} \ , \tag{3}$$

where

$$\mathbf{T}_k^{\mu} = \alpha_k \mu_k \left(\nabla \boldsymbol{u}_k + (\nabla \boldsymbol{u}_k)^T \right) \ , \tag{4}$$

and μ_k is molecular viscosity of phase k. Turbulent stress $\mathbf{T}_k^{\mathrm{T}}$ is obtained with the k-ω SST turbulence model (Menter et al., 2003). Momentum sources due to phase interaction

$$\boldsymbol{M}_k = \boldsymbol{F}_{kq}^{\mathrm{D}} + \boldsymbol{F}_{kq}^{\sigma} \tag{5}$$

consist of the interphase drag force $\boldsymbol{F}_{kq}^{\mathrm{D}}$, which models the transfer of momentum between the phases k and q, and the surface tension force $\boldsymbol{F}_{kq}^{\sigma}$.

The system of equations is solved using the PIMPLE algorithm for pressure–velocity coupling. The PIMPLE algorithm (The OpenFOAM Foundation Ltd, 2020) is a combination of PISO (Pressure Implicit with Splitting of Operator) and SIMPLE (Semi-Implicit Method for Pressure-Linked Equations). Inner PISO iterations comprise the solution of pressure equation and momentum corrector. They are combined with outer SIMPLE iterations, which involve all steps of the solution procedure inside each single time step including transport equations for fields of phase fractions and turbulent quantities. In that way, the coupling between the various solution variables of the underlying multi-field two-fluid model can be reflected in the solution procedure. In the course of this work three outer and two inner iterations turned out to deliver a reliable numerical solution with reasonable computational effort and, therefore, are the chosen numerical parameters. Momentum and turbulent transport equations are discretized second order accurate in space and first order implicit in time. The numerical diffusion of the large interface is limited by using the interface compression algorithm of Weller (2008). Adaptive time stepping was used to perform transient simulations with the Courant number set to a target value of 0.5.

2.2. Surface tension force

The continuum surface force model of Brackbill et al. (1992) is used to model the surface tension

$$\boldsymbol{F}_{kq}^{\sigma} = \alpha_k \sigma_{kq} \kappa_{kq} \widehat{\mathbf{n}}_{kq} \ . \tag{6}$$

The interface curvature is given by

$$\kappa_{kq} = \nabla \cdot \widehat{\mathbf{n}}_{kq} \ , \tag{7}$$

where normal to the interface is calculated from the volume fraction gradient as

$$\widehat{\mathbf{n}}_{kq} = \frac{\nabla \alpha}{|\nabla \alpha|} \ . \tag{8}$$

The surface tension coefficient is $\sigma_{kq} = 0.072\,\mathrm{N/m}$ for the air–water system.

2.3. Interphase drag force

A no-slip interfacial condition can be assumed at an interface between a pair of incompressible fluids in two-phase flow without phase change (Tryggvason et al., 2011), such as the stratified flow considered in the present work. In the single-fluid formulation with one common velocity field (the homogeneous model), the phase velocities at the interface are equal by definition. Within the two-fluid model formulation, with multiple coexisting velocity fields, Štrubelj and Tiselj (2010) introduced a numerical drag force to be used for a resolved interface between continuous phases

$$\boldsymbol{F}_{kq}^{\mathrm{D}} = \frac{\alpha_k \alpha_q \rho_{kq}}{\tau_r} \left(\boldsymbol{u}_q - \boldsymbol{u}_k \right) \ , \tag{9}$$

where τ_r is the relaxation time and $\rho_{kq} = (\alpha_k \rho_k + \alpha_q \rho_q)/(\alpha_k + \alpha_q)$ the weighted density of phase pair k and q. The recommended value for τ_r is orders of magnitude smaller than the simulation time step size (Štrubelj and Tiselj, 2010). In the present work, the relaxation time is set to $\tau_r = 10^{-8}\Delta t$ to ensure a strong coupling of phase velocities at the interface.

When larger interfacial structures are modelled in an under-resolved manner, i.e., when the computational grid is not sufficient to resolve all interfacial structures or turbulent scales, it can be more appropriate to model some tangential velocity slip at the interface (Meller et al., 2020; Gauss et al., 2016). Here, the use of the two-fluid model formulation for large interfacial structures is more flexible compared to the simpler homogeneous model, as different drag correlations can be applied.

As will be shown later via the results presented in this paper (see Section 3), a reasonable agreement between simulation and experimental observations (Stäbler, 2007) can be obtained already with the simplest no-slip assumption using the drag force from Eq. (9). Therefore, more accurate (and complex) drag force models used by other authors (Coste, 2013; Höhne and Mehlhoop, 2014; Porombka and Höhne, 2015; Mathur et al., 2019) for turbulent stratified flows are not investigated in the present work.

2.4. Turbulence damping at the gas–liquid interface

To improve turbulence modelling near the gas–liquid interface in stratified flow, the capabilities of the presently used solver are augmented with the turbulence damping method based on the model originally proposed by Egorov (2004). In this approach, additional damping terms are added to turbulence equations (for example ω equation of the k-ω RANS model), which mimic the wall-like damping of turbulence near an interface, as reported by Fulgosi et al. (2003).

In the present work, the turbulence damping term S_k^{ω} was added to the ω_k-transport equation of the k-ω SST turbulence model (Menter et al., 2003)

$$\begin{aligned} \frac{\partial}{\partial t}(\alpha_k \rho_k \omega_k) + \nabla \cdot (\alpha_k \rho_k \boldsymbol{u}_k \omega_k) = \nabla \cdot \left(\alpha_k \left(\mu_k + \sigma_\omega \mu_k^T \right) \nabla \omega_k \right) + \frac{\alpha_k \rho_k \gamma}{\mu_k^T} \widetilde{P}_k \\ - \beta \alpha_k \rho_k \omega_k^2 + 2(1 - F_1) \frac{\alpha_k \rho_k \sigma_{\omega 2}}{\omega_k} (\nabla k_k) \cdot (\nabla \omega_k) + S_k^{\omega} \ . \end{aligned} \tag{10}$$

Here, μ_k and μ_k^T are the dynamic and eddy viscosities, respectively, and k_k is the turbulent kinetic energy. Terms $\beta, \sigma_\omega, \sigma_{\omega 2}, \gamma, F_1$ are the model coefficients and $\widetilde{P}_k$ is the turbulent kinetic energy production term of the k-ω SST model (Menter et al., 2003).

The turbulence damping term S_k^{ω} counteracts the destruction term for dissipation rate $-\beta \alpha_k \rho_k \omega_k^2$ in Eq. (10), imposing a large (wall-like) value for ω_k at the interface, and thus damping the turbulent kinetic energy (Egorov, 2004). In the present work, the expression of Frederix et al. (2018) with damping length scale δ_k is adopted for the damping term

$$S_k^{\omega} = A \alpha_k \beta \rho_k \left(\frac{\nu_k}{\beta \delta_k^2} \right)^2 \ , \tag{11}$$

where A is the interface indicator field, $\nu_k = \mu_k/\rho_k$ is the phase kinematic viscosity and β is the coefficient of the k-ω SST model.

The purpose of the indicator field A is to apply turbulence damping in the vicinity of the interface. For this purpose, the limited indicator function is defined as

$$A = \min\left(a_{kq}\Delta, 1\right), \tag{12}$$

where the interfacial area density a_{kq} between phases k and q is calculated as

$$a_{kq} = \left| \alpha_q \nabla \alpha_k - \alpha_k \nabla \alpha_q \right| \ , \tag{13}$$

and the typical mesh size normal to the interface is approximated as

$$\Delta = \begin{cases} \sqrt[2]{V_c/l_z} \ , & \text{for a 2D mesh} \\ \sqrt[3]{V_c} \ , & \text{for a 3D mesh} \end{cases} \tag{14}$$

where l_z is the depth of a 2D domain and V_c is the local cell volume.

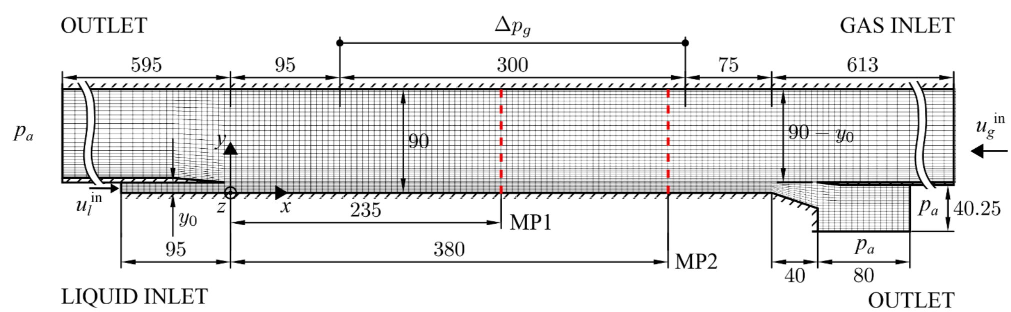

Fig. 1. Computational domain and boundary conditions. All dimensions are in mm. Cells of the two-dimensional Mesh 1 from Table 1 are shown here for illustration. The three-dimensional domain has been uniformly extruded in z-direction with a d.epth of 110 mm.

Table 1
2D mesh cell sizes for the channel section.

	Δx [mm]	$\Delta y_{\mathrm{water}}$ [mm]	Δy_{air} [mm]	N_{cells} [−]
Mesh 1	5.00	1.00	2.60	8002
Mesh 2	2.50	0.50	1.30	32557
Mesh 3	1.25	0.25	0.65	130528

Table 2
3D mesh cell sizes for the channel section

Δx [mm]	$\Delta y_{\mathrm{water}}$ [mm]	Δy_{air} [mm]	Δz [mm]	N_{cells} [−]
5.00	1.00	2.60	5.00	176044

Table 3
Flow properties.

	ρ_k [kg/m^3]	μ_k [Pa·s]	u_k^{in} [m/s]	Re_k [−]
Air	1.20	$1.82 \cdot 10^{-5}$	4.44	$2.73 \cdot 10^4$
Water	998	$1.00 \cdot 10^{-3}$	0.70	$1.16 \cdot 10^4$

2.5. Computational domain and mesh

The chosen computational domain represents the test section part of the WENKA experimental facility (Stäbler et al., 2006) and is shown in Fig. 1. Vertical profiles of volume fraction, velocity and turbulence fields were measured at two streamwise positions, which are indicated as MP1 and MP2. Measurements of the pressure difference in the gas phase were performed between locations marked with Δp_g. The height of the water inlet channel is indicated as $y_0 = 9$ mm.

Two-dimensional simulations were performed by using a single mesh cell in the third direction with a depth of 1 mm. The actual depth of the WENKA test section of 110 mm was used only for the three-dimensional domain simulations. A hexahedral mesh, such as the one shown in Fig. 1, was used.

Tables 1 and 2 show the prescribed cell sizes in the channel section of the domain ($-5\,\mathrm{mm} \leqslant x \leqslant 470\,\mathrm{mm}$, see Fig. 1) for the two- and three-dimensional simulations, respectively. In the gas outlet and inlet regions, the streamwise division was gradually increased to the value of $2\Delta x$. Table 1 shows that different cell heights were used in the water region ($y < 9$ mm) and air region ($y > 9$ mm) of the channel. However, cells were refined on both sides to match in size and to have a smooth transition from smaller water cells to larger air cells. Additionally, cells were refined slightly near the channel upper and lower walls to improve the mesh resolution in the wall boundary layer. For the three-dimensional simulations, the 2D mesh configuration shown in Fig. 1 is extruded uniformly in z-direction with a depth of 110 mm. This direction is resolved with 22 cells with size $\Delta z = 5$ mm, as listed in Table 2.

Table 4
Turbulence initial conditions.

	I_k [−]	μ_k^T/μ_k [−]	k_k [m^2/s^2]	ω_k [1/s]
Air	0.05	10	$7.39 \cdot 10^{-2}$	488
Water	0.05	10	$1.84 \cdot 10^{-3}$	183

2.6. Boundary and initial conditions

Table 3 shows properties of air and water, which are based on flow conditions 3 and 23 of the WENKA experiment (Stäbler, 2007). Water enters the channel at the liquid inlet on the bottom left (as indicated in Fig. 1), flows through the test section and drains over a ramp at the bottom-right end of the domain. Air enters at the gas inlet on the right side of the domain and flows through the channel counter-currently to the water. A nearly steady-state supercritical (Fr $= 2.36$) stratified flow develops in the channel with only small ripple waves and thus a relatively smooth and well defined interface between air and water is established. These conditions are commonly used for validation of stratified flow models in literature (Porombka and Höhne, 2015; Höhne and Porombka, 2018). Here, the height of liquid film at the inlet ($y_0 = 9$ mm) is used to calculate the Froude number (Porombka and Höhne, 2015)

$$\mathrm{Fr} = \frac{u_l^{\mathrm{in}}}{\sqrt{g \cdot y_0}} = 2.36\ . \tag{15}$$

The Reynolds numbers (see Table 3) of each phase are based on the mean velocity magnitude at the inlet (u_k^{in}) and the hydraulic diameter (d_k)

$$\mathrm{Re}_k = \frac{\rho_k u_k^{\mathrm{in}} d_k}{\mu_k}\ . \tag{16}$$

Profiles of velocity at the water and air inlet boundaries are not known from the experiment and have to be estimated from their respective mean magnitude values. For this purpose, field mapping from locations further downstream was used to obtain the profiles of velocity and turbulence fields of a fully developed channel flow at the individual phase inlets. Mapped values were sampled from cross-sectional planes located 45 mm from the water inlet and 493 mm from the air inlet boundary. Table 3 shows the imposed constrains on mean values for mapped velocity fields at air and water inlets, respectively. Turbulence fields were mapped without imposed constraints. The phase specific velocities are set to be identical at each individual inlet boundary, e.g. using the value of u_g^{in} for both air and water velocity at air inlet, and similarly using u_l^{in} for both velocities at water inlet. No-slip boundary conditions are imposed at channel walls. Flows of pure air and water are imposed at air and water inlets, respectively. At both outlets, fixed-value conditions are applied to the pressure field, while zero-gradient conditions are used for the remaining fields, namely phase-specific velocity fields, phase fraction fields and fields of turbulent properties.

Initial phase-specific velocity fields were set to zero and the initial pressure was set to the ambient pressure of 100900 Pa (Stäbler, 2007). Fields of phase-specific turbulent kinetic energy k_k and specific dissipation rate ω_k were set to their respective initial values shown in Table 4. Values of initial turbulent kinetic energy for both water and air were estimated from the turbulence intensity I using

$$k_k^{\mathrm{in}} = \frac{3}{2}\left(u_k^{\mathrm{in}} I_k\right)^2 . \tag{17}$$

The specific dissipation rate was estimated assuming the ratio of eddy and molecular viscosity $\mu_k^T/\mu_k = 10$ and using

$$\omega_k = \frac{\rho_k k_k}{\mu_k}\left(\frac{\mu_k^T}{\mu_k}\right)^{-1} . \tag{18}$$

At the start of the simulation, the part of the channel between the water inlet and left tip (at $x = -5$ mm) is filled with water, while the rest of domain is full of air. During the simulation, water, which enters the domain at the left inlet, flows through the test section and drains over a ramp at the bottom-right end.

After initial perturbation, a nearly steady stratified counter-current flow of air and water develops in the simulated channel. But, as very small oscillations in the flow were observed (as demonstrated for the pressure difference results in Section 3.1) the time averaged flow fields are investigated. After the initial transient, the flow was averaged over a time period of 10 s, which is equivalent to about 14 flow-through times of the channel test section (length of 0.470 m) based on the mean water velocity of 0.7 m/s.

3. Results and discussion

The goal of the results presented in this section is to demonstrate the capabilities of the hybrid model framework (Meller et al., 2020) to adequately model the turbulent flow conditions near a smooth gas–liquid interface in isothermal counter-current stratified flow. Simulation results are compared to measurement data from WENKA

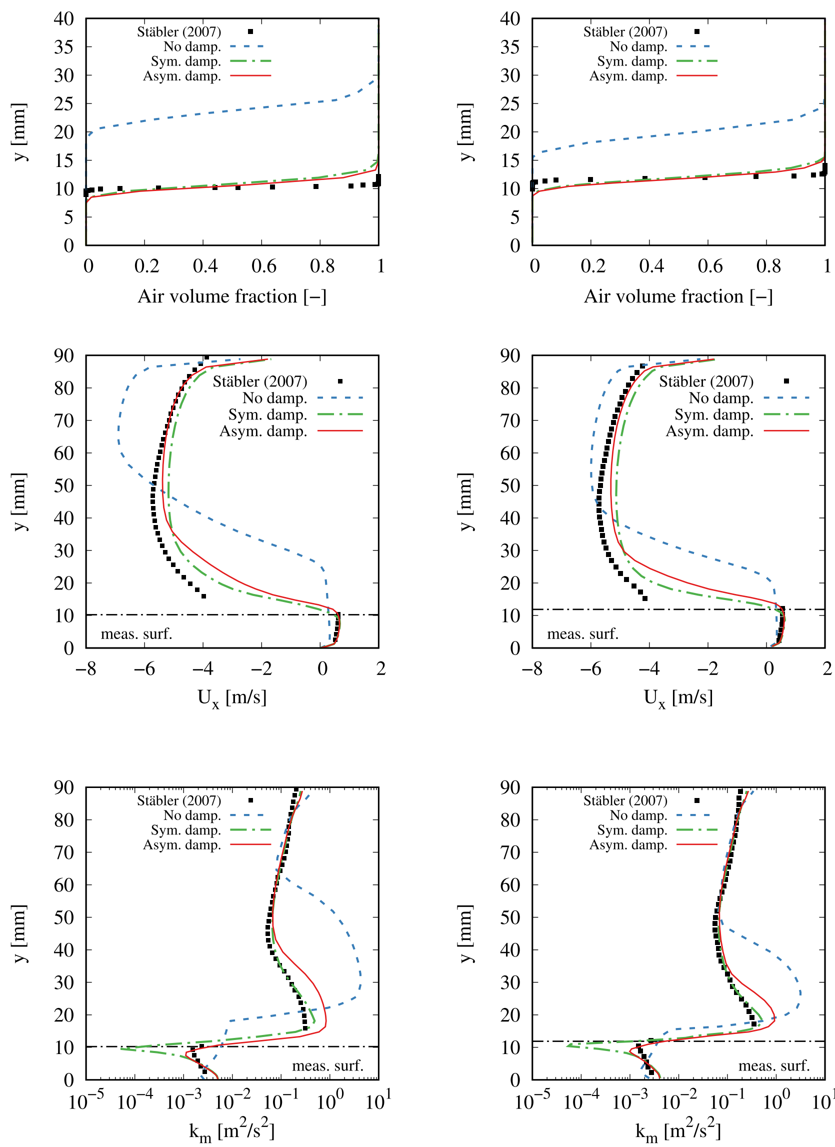

(a) MP1 (b) MP2

Fig. 2. Comparison between measurement data (Stäbler, 2007) and simulations with different damping strategies: no damping, symmetric (both phases) and asymmetric (only in the gas phase). The horizontal dash-dot line shows the water level measured in. the experiment.

experiment (Stäbler, 2007), which include vertical profiles of phase volume fraction, velocity and turbulent kinetic energy, as well as the pressure difference in the test channel.

Presented results are organized into four sets. The first set represents an evaluation of different turbulence damping approaches: no damping, symmetric damping (both phases) and asymmetric damping (only the gas phase). The second set shows results of a parametric study on the damping length scale parameter δ_k, which affects the amount of damping of the turbulent kinetic energy near an interface. These simulations were performed using the coarse two-dimensional mesh 1 (see Table 1). Hence, the third set represents the results of mesh sensitivity study using the asymmetric damping approach. Finally, results of simulations using a three-dimensional domain (see Table 2) are shown, which represents the actual channel geometry in the WENKA experiment more precisely.

3.1. Evaluation of the turbulence damping approach

The results presented in this section illustrate the necessity for turbulence damping near the interface in RANS modelling of stratified flows. Data marked with *no damping* were obtained without the damping term given by Eq. (11). Simulations with *symmetric damping* were performed with damping terms present in turbulence models for both phases using identical values for the damping length scale parameter (with $\delta_g = \delta_l = 7{\cdot}10^{-5}$ m). Simulations with *asymmetric damping* were performed with the damping term being only present in the gas phase.

The damping length scale parameter value can be determined from the parameters used by Porombka and Höhne (2015), who simulated the WENKA experiment with the AIAD model using the original damping formulation by Egorov (2004), which is formulated in terms of damping coefficient $B = 100$ and grid spacing parameter $\Delta n = 1.65\,\mathrm{mm}$. The damping length scale was then obtained using the definition of damping scale parameter $\delta_k^2 = \Delta n^2/(6B)$ adopted from the paper of Frederix et al. (2018).

Simulation results for vertical profiles of air volume fraction, mixture streamwise velocity U_x and mixture turbulent kinetic energy $k_m = \alpha_g k_g + \alpha_l k_l$ are presented in Fig. 2 and compared with measured profiles provided by Stäbler (2007). The profiles of turbulent kinetic energy show the modelled values obtained from the k-ω SST turbulence model. Phase velocity fields coexist in the two-fluid model as “interpenetrating continua” in each point in space and time (Ishii and Hibiki, 2006). The mixture velocity of pure gas and liquid regions in stratified flows is equal to the respective velocity of the present phase. These two regions are separated by an interface, represented in the two-fluid model as a band of cells, where phase volume fractions are between 0 and 1. The drag force model (see Eq. (9)) ensures the strong momentum coupling, which essentially equalises the phase velocities (fulfilling the no-slip condition at the interface). Hence, it is sufficient to plot only the velocity of one phase (water in this case) for the vertical profiles over the whole domain. This is in contrast to other two-fluid model simulations of WENKA in the literature (Höhne and Mehlhoop, 2014; Höhne and Porombka, 2018), where velocity slip was permitted. Profile plots are extracted at the two locations in the channel, according to experimental investigations: MP1 at $x = 235\,\mathrm{mm}$ and MP2 at $x = 380\,\mathrm{mm}$ (also marked in Fig. 1). The horizontal dash-dot line in Fig. 2, annotated with *meas. surf.*, indicates the water surface level measured in the experiment (Stäbler, 2007).

When compared to the measured data (similarly as in Porombka and Höhne, 2015; Höhne and Porombka, 2018), profiles obtained without turbulence damping show much larger discrepancies and indicate that these simulations predict a different flow regime. Due to the large overestimation of liquid surface height, as indicated by the air volume fraction profile, and thus narrower flow area for the gas, the maximum velocity is significantly larger compared to simulations with damping or the experimental data. The second noticeable discrepancy is a smaller velocity gradient in the gas phase near the interface, due to the overprediction of turbulent kinetic energy and, hence, the increased exchange of momentum. For this reason, characteristic linear profiles of gas velocity above the interface are observed in the results without damping (see U_x profile in Fig. 2a for y between 30 and 50 mm). Similar observations were noted by other authors, who simulated the stratified flow in the WENKA channel (Porombka and Höhne, 2015; Höhne and Porombka, 2018), although they used a different drag force model (AIAD) and different turbulence damping formulation (with original Egorov term) compared to the present modelling approach.

As demonstrated by the results in Fig. 2, the prediction of measured vertical profiles improves significantly with symmetric damping. However, similarly to observations in the literature (Höhne and Porombka, 2018; Porombka and Höhne, 2015; Frederix et al., 2018), the turbulence damping procedure tends to underpredict the values of turbulent kinetic energy on the liquid side of the interface. Trying to alleviate this problem, Höhne and Porombka (2018) used an additional turbulence production term by introducing the sub-grid wave turbulence model (SWT) and disabled the damping term in the liquid phase. They found that the effect of the SWT model is very small for the simulated flow conditions, with only small ripple waves present. When both approaches are used, it is also difficult to distinguish between the effects of the SWT model and the disabled damping term. For this reason, the SWT model was not considered in the present work. Present comparison of the results between symmetric and asymmetric damping indicates that asymmetric damping improves the prediction of turbulent kinetic energy on the liquid side of the interface, as shown in Fig. 2. But, as also noted by Höhne and Porombka (2018), it comes with the cost of a worse prediction of streamwise velocity and, to a lesser extent, turbulent kinetic energy on the gas side of the interface.

In addition to vertical profiles of the flow, the pressure difference Δp_g in the gas part of the channel (see Fig. 1) was measured to be 0.8 ± 0.6 Pa for the simulated flow conditions of the WENKA experiment (Stäbler, 2007). Fig. 3 shows the simulated pressure difference Δp_g over time for simulations with symmetric and asymmetric turbulence damping. As shown, the only noticeable difference are the larger oscillations in pressure for the symmetric case. After the initial transient, the pressure difference converges within the measured tolerance in both cases. For simulations without dampening, the pressure difference was at least an order of magnitude higher compared to the measured one and is therefore not shown in Fig. 3.

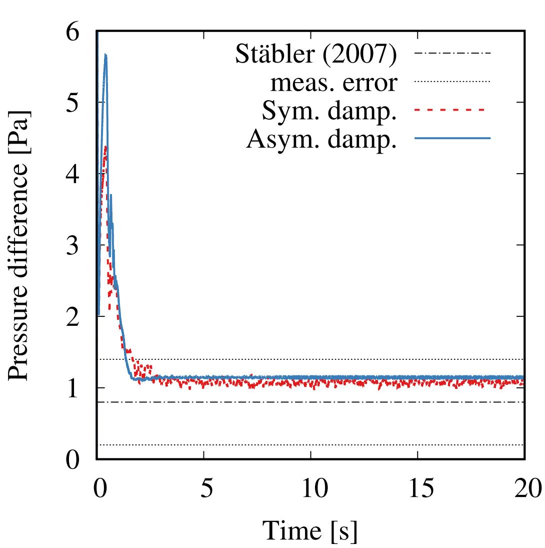

Fig. 3. Simulated pressure difference Δp_g using symmetric and asymmetric turbulence damping compared with experimental results of Stäbler (2007).

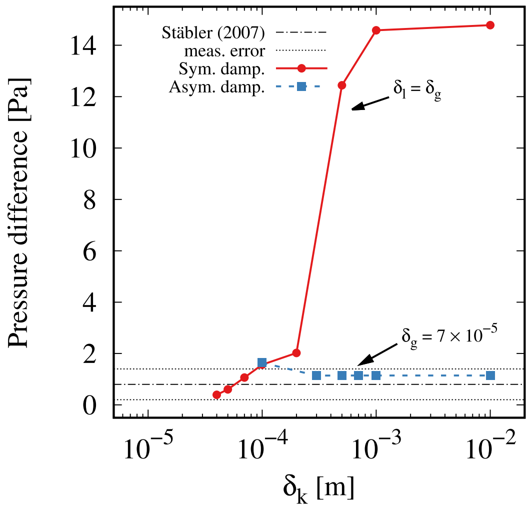

Fig. 4. Simulated pressure difference Δp_g using different turbulence damping scales compared with experimental results of Stäbler (2007).

3.2. Parametric study on the turbulence damping scale

The amount of turbulence damping (the strength of S_k^ω term in Eq. (11)) is controlled by the damping scale parameter δ_k, of which the physical interpretation is an open subject in the literature (Frederix et al., 2018; Mathur et al., 2019). Frederix et al. (2018) presented a parametric study for the co-current stratified flow in channel experiment of Fabre et al. (1987) over a range of damping scale values from approximately 10^{-2} m to 10^{-5} m and recommended the value of 10^{-4} m to be used.

A similar parametric study is performed in the present work on the counter-current stratified flow case from the WENKA experiment. The objective is to investigate if the damping scale formulation performs consistently on a different stratified flow case. In addition to symmetric damping ($\delta_g = \delta_l$), the present parametric study is performed using asymmetric damping, where weaker damping is prescribed with a larger damping scale $\delta_l > \delta_g$ on the liquid side. Here, the definition of asymmetric damping used in the previous section is extended, as very large values of δ_l mean that the damping term in liquid is essentially disabled ($S_k^\omega \rightarrow 0$ in Eq. (11)). For symmetric damping, values from $\delta_k = 10^{-2}$ m down to $4 \cdot 10^{-5}$ m are investigated. For asymmetric damping, different liquid damping scale values from $\delta_l = 10^{-2}$ m down to 10^{-4} m are investigated, while a constant value $\delta_g = 7 \cdot 10^{-5}$ m is used in the gas phase. The idea behind using different asymmetric damping scale values is to investigate if a small amount of turbulence damping in liquid phase (in contrast to no damping) could further improve simulation results.

Fig. 4 shows the results for the pressure difference using different values for symmetric and asymmetric damping scales. Results demonstrate a transition region between δ_k values of 10^{-4} m and 10^{-3} m where a steep increase in simulated pressure difference occurs, which indicates a significant change in the simulated flow pattern. The observed transition band agrees with the one reported by Frederix et al. (2018) for the simulations of co-current stratified flow in the channel of Fabre et al.

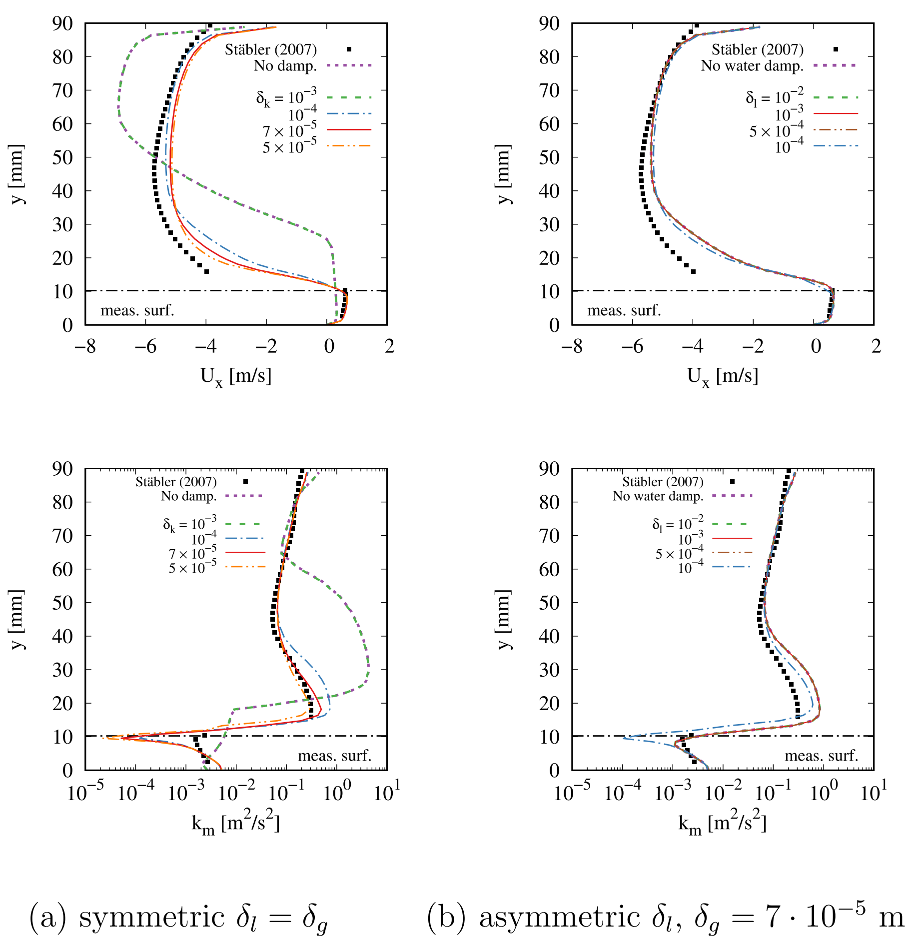

Fig. 5. Comparison between different profiles at MP1 ($x = 235$ mm) using symmetric and asymmetric damping scales. The horizontal dash-dot line shows the water level measured in the experiment (Stäbler, 2007).

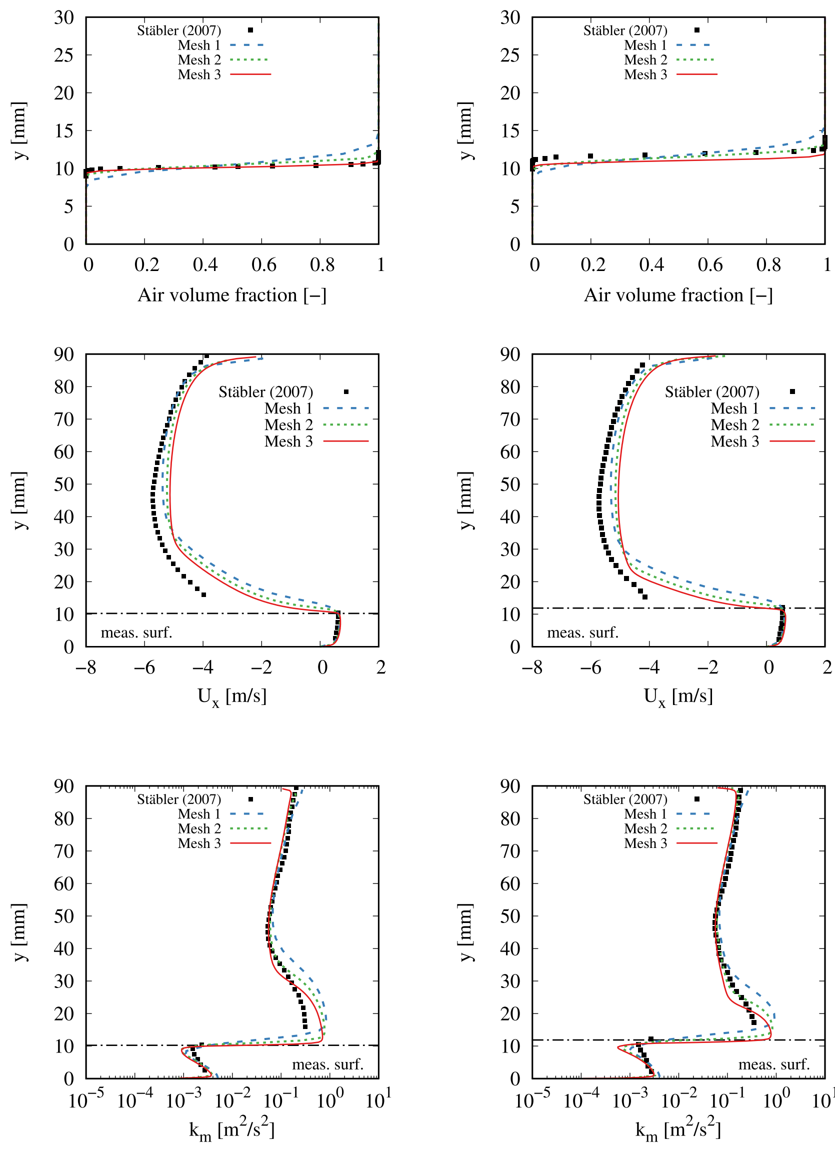

(a) MP1   (b) MP2

Fig. 6. Mesh study for simulations using asymmetric turbulence damping. The horizontal dash-dot line shows the water level measured in the experiment (Stäbler, 2007).

(1987). For symmetric damping scales below the recommended value of $\delta_k = 10^{-4}$ m (Frederix et al., 2018), calculated pressure differences fall within the measured error band. The second set of results with the asymmetric approach display only a very small variation with different damping scale values δ_l in the liquid phase (at constant value in the gas phase).

Next, the effects of different damping scale values on the simulated vertical profiles of the flow are investigated. Fig. 5 shows comparison of different vertical profiles at MP1 using different values for symmetric and asymmetric damping scales δ_k and also including simulation without any damping. Evidently, the results without damping or with large damping scales above the transition region are significantly different to the ones where the damping scale is close to or smaller than the recommended value of 10^{-4} m.

With symmetric damping, small improvements can be observed with decreasing damping scale values, as shown by the vertical profiles in Fig. 5a. At the same time, results show that the error in the underprediction of turbulent kinetic energy near the interface is increasing with the diminishing damping scale. The value of $\delta_k = 7\cdot 10^{-5}$ m seems to offer a good compromise and is only slightly smaller that the value of 10^{-4} m recommended by Frederix et al. (2018).

As can be derived from the study on pressure difference (both in Fig. 4 and in Frederix et al., 2018), the damping scale parameter acts similarly to an on/off switch with a transition band between 10^{-4} m and 10^{-3} m (and is very similar to the results of Frederix et al., 2018) for turbulence damping. This is especially evident for asymmetric damping in Fig. 5b, where the results for $\delta_l < 10^{-4}$ m are essentially the same as the one where damping in water was turned off by removing the source term. Thus, the study on using different asymmetric damping values in the liquid phase did not produce any improvement of the simulated profiles, compared to the ones presented in the previous Section 3.1.

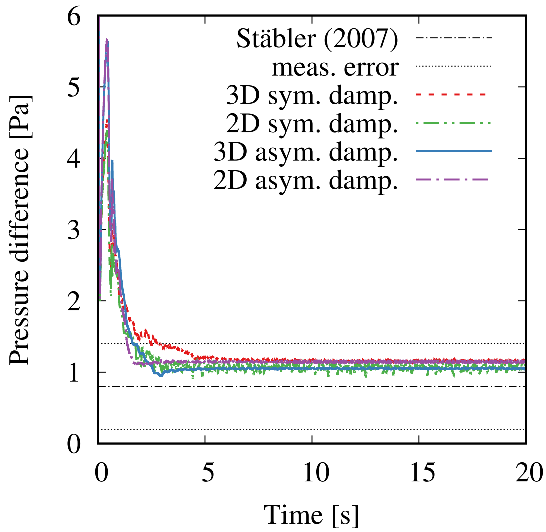

Fig. 7. Simulated pressure difference Δp_g on 3D mesh compared to 2D results and measurements (Stäbler, 2007).

3.3. Mesh sensitivity study

The present modelling approach is evaluated further with a mesh sensitivity study performed using three different two-dimensional meshes (see Table 1) and and the asymmetric damping approach with $\delta_g = 7{\cdot}10^{-5}$ m and no damping in water. Results for vertical profiles are presented in Fig. 6 and show reasonable agreement between different meshes. At the location MP1, the volume fraction profiles are converging towards the measured ones. At the second location MP2, the water level is slightly under-predicted, especially on Mesh 3. Volume fraction profiles reveal that the interface is resolved more accurately on finer meshes compared to coarser ones. This has an effect on the vertical profiles for velocity and turbulent kinetic energy near the gas–liquid interface, which exhibit higher gradients in the interface region as well.

Small differences between meshes can also stem from the fact, that the strength of the turbulence damping source from Eq. (11) is affected by the magnitude of the interface indicator field in Eq. (12), which includes the approximation of local grid size normal to the interface in Eq. (14). As shown before with the parametric study on the damping scale (see Fig. 5), the strength of the turbulence damping source has a small effect on velocity profiles.

3.4. Three-dimensional simulation

The two-dimensional meshes are used to perform the parametric study on turbulent damping scale. However since depth (110 mm) and height (90 mm) of the WENKA test section are quite comparable, and side walls of the channel can have an effect on the flow in the middle plane (where measurements were taken), a full three-dimensional simulation represents a more realistic setup for validation. The numerical model and procedure used for 2D simulations are applied to the 3D simulation with mesh parameters listed in Table 2. Again, the symmetric damping ($\delta_g = \delta_l = 7{\cdot}10^{-5}$ m) and asymmetric damping approach (without damping in the liquid phase) were investigated. For the 3D simulations, the near wall mesh resolution corresponds to the maximum y^+ value of 24 at both top and bottom walls of the channel test section (the region between $-5\,\text{mm} \leqslant x \leqslant 470\,\text{mm}$, see Fig. 1) for air and water,

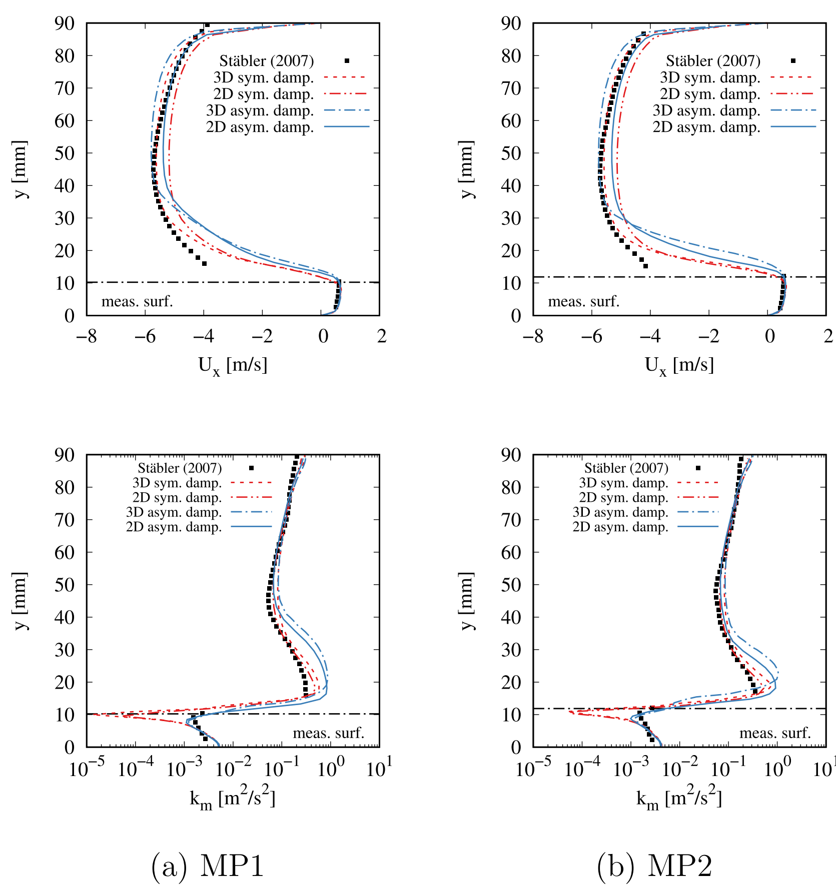

Fig. 8. Results for a 3D domain compared to 2D domain results and measured vertical profiles by Stäbler (2007). The horizontal dash-dot line shows the water level measured in the experiment.

respectively.

Regarding the pressure difference in the gas phase, results in Fig. 7 show no significant difference between 2D and 3D simulation when quasi steady state is reached after the initial transient. Both 3D results, with symmetric and asymmetric damping, are within the error band of the measured results by Stäbler (2007). Again, without damping the simulated pressure difference is significantly higher and, hence, it is not shown.

Fig. 8 shows results for vertical profiles of streamwise velocity and turbulent kinetic energy obtained with 3D simulations, which are compared with the 2D mesh results and the experimental measurements (Stäbler, 2007). Results regarding velocity values and especially the velocity maximum are improved when using a three-dimensional domain. Regarding profiles of turbulent kinetic energy obtained with symmetric damping, minor differences can be observed between 2D and 3D results, with better agreement of 2D results with the measured profile in the gas flow.

4. Summary and conclusions

The results presented in this paper demonstrate the capability of the hybrid model Meller et al. (2020) to simulate stratified flows. The solver is implemented in OpenFOAMC++ library and uses consistent momentum interpolation together with the partial elimination algorithm in order to handle strong momentum coupling implied by the no-slip assumption at the interface, which allows to mimic the behaviour of a homogeneous model. Turbulence damping at the free-surface with the damping scale formulation of Frederix et al. (2018) was introduced into the $k-\omega$ SST model in OpenFOAM and the implementation was tested and validated with measurements of the isothermal stratified air–water counter-current channel flow in the WENKA experiment (Stäbler et al., 2006; Stäbler, 2007). Validation results include comparisons of pressure difference in the channel and vertical profiles of volume fraction, velocity and turbulent kinetic energy.

Symmetric and asymmetric damping were investigated, where turbulence damping is applied in both phases and solely in the gas phase, respectively. Asymmetric damping improves the prediction of turbulent kinetic energy on the liquid side of the interface, but with the cost of reducing accuracy of velocity profiles on the gas side. With symmetric damping, the turbulent kinetic energy near the interface tends towards very small values, which is not observed in the experiment.

A parametric study on the damping scale parameter was performed and the obtained behaviour of the model is comparable to findings presented by Frederix et al. (2018) for their simulations of the co-current stratified flow in the Fabre channel (Fabre et al., 1987). The damping scale acts similar to an on/off switch with a transition band between values 10^{-3} and 10^{-4} m (the latter being the recommended value by Frederix et al. (2018)). Present simulations show that a slightly smaller value of $\delta_k = 7\cdot10^{-5}$ m, which was derived from Egorov damping parameters in AIAD simulations of WENKA channel by Porombka and Höhne (2015), yields better agreement between simulated and measured flow data. On the other hand, the investigation with less damping prescribed in the liquid phase compared to the gas phase ($\delta_l > \delta_g$) did not produce any improvement over the results where the damping term in water was completely removed, as proposed by Höhne and Porombka (2018).

Finally, using the most appropriate asymmetric damping strategy determined with the 2D parametric study, three-dimensional simulations of the WENKA test section were performed. These results show that slight improvements in the prediction of the velocity profiles in the gas phase can be obtained with a more realistic 3D model.

In view of the morphology adaptive framework (Meller et al., 2020), present results validate the no-slip drag force approach (mirroring homogeneous model) with turbulence damping on a stratified flow case with a relatively smooth interface. More complex stratified flow cases, with unresolved surface waves and droplets, will require future improvements in the drag force modelling approach (allowing some velocity slip) and ability to handle disperse phase entrainment and deentrainment processes, that can occur when waves mix and break.

CRediT authorship contribution statement

Matej Tekavčič: Conceptualization, Methodology, Software, Investigation, Writing - original draft, Visualization. **Richard Meller:** Methodology, Software, Writing - review & editing, Validation. **Fabian Schlegel:** Conceptualization, Methodology, Writing - review & editing, Supervision, Project administration.

Declaration of Competing Interest

The authors declare that they have no known competing financial interests or personal relationships that could have appeared to influence the work reported in this paper.

Acknowledgements

This work was supported by the Helmholtz European Partnering Program in the project “Crossing borders and scales (Crossing)”. The author from the Jožef Stefan Institute gratefully acknowledges also the financial support provided by the Slovenian Research Agency through the grant P2-0026.

References

Apanasevich, P., 2019. Analysis and Modelling of Heat and Mass Transfer in Two-Phase Counter-Current Condensing Flows at High Pressure using Direct Numerical and Highly-Resolved Large Eddy Simulations. Ph.D. thesis. Technische Universität Dresden.

Barna, I.F., Imre, A.R., Baranyai, G., Ézsöl, G., 2010. Experimental and theoretical study of steam condensation induced water hammer phenomena. Nucl. Eng. Des. 240, 146–150. https://doi.org/10.1016/j.nucengdes.2009.09.027.

Bestion, D., 2012. Applicability of two-phase CFD to nuclear reactor thermalhydraulics and elaboration of best practice guidelines. Nucl. Eng. Des. 253, 311–321. https://doi.org/10.1016/j.nucengdes.2011.08.068.

Bestion, D., 2014. The difficult challenge of a two-phase CFD modelling for all flow regimes. Nucl. Eng. Des. 279, 116–125. https://doi.org/10.1016/j.nucengdes.2014.04.006.

Brackbill, J.U., Kothe, D.B., Zemach, C., 1992. A continuum method for modeling surface tension. J. Comput. Phys. 100, 335–354. https://doi.org/10.1016/0021-9991(92)90240-y.

Coste, P., 2013. A large interface model for two-phase CFD. Nucl. Eng. Des. 255, 38–50. https://doi.org/10.1016/j.nucengdes.2012.10.008.

Cubero, A., Sánchez-Insa, A., Fueyo, N., 2014. A consistent momentum interpolation method for steady and unsteady multiphase flows. Comput. Chem. Eng. 62, 96–107. https://doi.org/10.1016/j.compchemeng.2013.12.002.

Egorov, Y., 2004. Validation of CFD codes with PTS-relevant test cases. Technical Report. EVOL-ECORA-D07, pp. 102–115.

Fabre, J., Suzanne, C., Masbernat, L., 1987. Experimental data set no. 7: stratified flow, part I: local structure. Multiphase Sci. Technol. 3, 285–301. https://doi.org/10.1615/multscientechn.v3.i1-4.120.

Frederix, E., Mathur, A., Dovizio, D., Geurts, B., Komen, E., 2018. Reynolds-averaged modeling of turbulence damping near a large-scale interface in two-phase flow. Nucl. Eng. Des. 333, 122–130. https://doi.org/10.1016/j.nucengdes.2018.04.010.

Fulgosi, M., Lakehal, D., Banerjee, S., Angelis, V.D., 2003. Direct numerical simulation of turbulence in a sheared airwater flow with a deformable interface. J. Fluid Mech. 482, 319–345. https://doi.org/10.1017/s0022112003004154.

Gauss, F., Lucas, D., Krepper, E., 2016. Grid studies for the simulation of resolved structures in an eulerian two-fluid framework. Nucl. Eng. Des. 305, 371–377. https://doi.org/10.1016/j.nucengdes.2016.06.009.

Hänsch, S., Lucas, D., Krepper, E., Höhne, T., 2012. A multi-field two-fluid concept for transitions between different scales of interfacial structures. Int. J. Multiph. Flow 47, 171–182. https://doi.org/10.1016/j.ijmultiphaseflow.2012.07.007.

Hänsch, S., Draw, M., Evdokimov, I., Khan, H., Krull, B., Lehnigk, R., Liao, Y., Lyu, H., Meller, R., Schlegel, F., Tekačič, M., 2021. HZDR Multiphase Case Collection for OpenFOAM. https://doi.org/10.14278/rodare.812, doi: 10.14278/rodare.812.

Höhne, T., Mehlhoop, J.P., 2014. Validation of closure models for interfacial drag and turbulence in numerical simulations of horizontal stratified gas–liquid flows. Int. J. Multiph. Flow 62, 1–16. https://doi.org/10.1016/j.ijmultiphaseflow.2014.01.012.

Höhne, T., Porombka, P., 2018. Modelling horizontal two-phase flows using generalized models. Ann. Nucl. Energy 111, 311–316. https://doi.org/10.1016/j.anucene.2017.09.018.

Ishii, M., Hibiki, T., 2006. Thermo-Fluid Dynamics of Two-Phase Flow. Springer, US. https://doi.org/10.1007/978-0-387-29187-1.

Kirsner, W., 1999. Steam condensation induced waterhammer. HPAC Heating/ Piping/ Air-Conditioning 71 (1), 112–124.

Lucas, D., Bestion, D., Bodèle, E., Coste, P., Scheuerer, M., D'Auria, F., Mazzini, D., Smith, B., Tiselj, I., Martin, A., Lakehal, D., Seynhaeve, J.M., Kyrki-Rajamäki, R., Ilvonen, M., Macek, J., 2009. An overview of the pressurized thermal shock issue in the context of the NURESIM project. Sci. Technol. Nucl. Installations 2009, 1–13. https://doi.org/10.1155/2009/583259.

Mathur, A., Dovizio, D., Frederix, E., Komen, E., 2019. A hybrid dispersed-large interface solver for multi-scale two-phase flow modelling. Nucl. Eng. Des. 344, 69–82. https://doi.org/10.1016/j.nucengdes.2019.01.020.

Meller, R., Schlegel, F., Lucas, D., 2020. Basic verification of a numerical framework applied to a morphology adaptive multi-field two-fluid model considering bubble motions. Int. J. Numer. Meth. Fluids. https://doi.org/10.1002/fld.4907.

Menter, F.R., Kuntz, M., Langtry, R., 2003. Ten years of industrial experience with the SST turbulence model. Turbulence Heat and Mass Transfer 4, 625–632.

Porombka, P., Höhne, T., 2015. Drag and turbulence modelling for free surface flows within the two-fluid euler–euler framework. Chem. Eng. Sci. 134, 348–359. https://doi.org/10.1016/j.ces.2015.05.029.

Schlegel, F., Draw, M., Evdokimov, I., Hänsch, S., Khan, H., Lehnigk, R., Meller, R., Petelin, G., Tekavčič, M., 2021. HZDR Multiphase Addon for OpenFOAM.https://doi.org/10.14278/rodare.795.

Spalding, D.B., 1981. Numerical computation of multi-phase fluid flow and heat transfer, in: Von Karman Institute for Fluid Dynamics Numerical Computation of Multi-Phase Flows.

Štrubelj, L., Tiselj, I., 2010. Two-fluid model with interface sharpening. Int. J. Numer. Meth. Eng. 85, 575–590. https://doi.org/10.1002/nme.2978.

Stäbler, T.D., 2007. Experimentelle Untersuchung und physikalische Beschreibung der Schichtenströmung in horizontalen Kanälen. Ph.D. thesis. Universität Stuttgart. doi: 10.5445/IR/200068452.

Stäbler, T.D., Meyer, L., Schulenberg, T., Laurien, E., 2006. Turbulence structures in horizontal two-phase flows under counter-current conditions, in: Proceedings of FEDSM2006, ASME Joint U.S. - European Fluids Engineering Summer Meeting, July 17–20, Miami, FL.https://doi.org/10.1115/fedsm2006-98211.

The OpenFOAM Foundation Ltd., 2020. OpenFOAM-dev https://openfoam.org/. URL https://github.com/OpenFOAM/OpenFOAM-dev/. commit 3659fb4, March 6th 2020.

Tryggvason, G., Scardovelli, R., Zaleski, S., 2011. Direct Numerical Simulations of Gas-Liquid Multiphase Flows. Cambridge University Press.

Weller, H.G., 2008. A New Approach to VOF-based Interface Capturing Methods for Incompressible and Compressible Flow. Technical Report. OpenCFD Ltd., Report TR/HGW.